analytical chemistry

pubs.acs.org/ac Article

Submicron Particle and Cell Concentration in a Closed Chamber Surface Acoustic Wave Microcentrifuge

Asma Akther, Susan Marqus, Amgad R. Rezk,* and Leslie Y. Yeo

Cite This: *Anal. Chem.* 2020, 92, 10024−10032 Read Online

ACCESS | Metrics & More | Article Recommendations | Supporting Information

ABSTRACT: Preconcentrating particulate and cellular matter for their isolation or detection is often a necessary and critical sample preparation or purification step in many lab-on-a-chip diagnostic devices. While surface acoustic wave (SAW) microcentrifugation has been demonstrated as a powerful means to drive efficient particle concentration, this has primarily been limited to micron dimension particles. When the particle size is around 1 μm or below, studies on SAW microcentrifugation to date have shown that particle ring-like aggregates can only be obtained in contrast to the localized concentrated clusters that are obtained with larger particles. Considering the importance of submicron particles and bioparticles that are common in many real-world samples, we elucidate why previous studies have not been able to achieve the concentration of these smaller particles to completion, and we present a practical solution involving a novel closed chamber configuration that minimizes sample heating and eliminates evaporation to show that it is indeed possible to drive submicron particle and cell concentration down to 200 nm diameters with SAW microcentrifugation over longer durations.

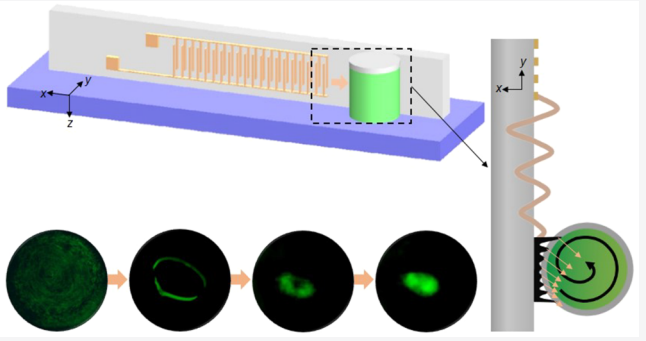

Downloaded via RMIT UNIV on May 17, 2021 at 23:53:46 (UTC).
See https://pubs.acs.org/sharingguidelines for options on how to legitimately share published articles.

Microparticle and nanoparticle concentration is an indispensable microfluidic operation in many lab-on-a-chip devices.[1,2] It is a critical sample preparation step, for example, for analyte enrichment to facilitate more sensitive detection in microfluidic biosensors, or it is an essential separation tool, for instance, for the purification of blood plasma from its cellular constituents in point-of-care medical diagnostic devices.[3] There are a number of ways by which the particle concentration can be effected to various extents in microfluidic devices, none of which are trivial, particularly given the typical difficulties associated with carrying out operations at microscale dimensions. These include inducing the particles to migrate and trap, either directly by applying a force on the particles or indirectly by using hydrodynamic forces that are localized within shear gradients or vortices.[4−7] Both of these direct and indirect microfluidic particle manipulation methods can be achieved under the influence of electric,[8−11] acoustic,[12−15] optical,[16,17] and magnetic fields.[18−21]

Acoustical systems offer a number of advantages for microfluidics, not least the sheer speeds at which microfluidic actuation can be driven.[12,22] Conventional bulk acoustic excitation typically driven at kHz frequencies, however, requires the use of large ultrasonic transducers, which are not always amenable for integration into a miniaturized format commensurate with portable point-of-care devices. These systems are also notorious for generating cavitation, which can be deleterious to biomolecules and cells. Their high-frequency (10 MHz order) surface counterpart, in the form of surface acoustic waves (SAWs; nanometer amplitude electromechanical Rayleigh waves)[23] and hybrid surface and bulk waves, known as surface reflected bulk waves (SRBWs),[24] offer a means to circumvent these limitations. Given their significantly higher fluid−structure coupling efficiency, these devices can be run at considerably lower powers that not only facilitate the use of miniaturized power sources that allow integration in a microfluidic setup but are also less likely to generate cavitation at high frequencies.[14] As such, SAWs are now a mainstay technology for driving a wide range of microfluidic actuation.[14,25−27]

To this effect, SAWs have been employed in microfluidic particle concentration both directly through the application of an acoustic radiation force on the particle as well as indirectly through the generation of localized vortices. In the former, both micron and submicron particles as well as cells can be trapped and hence concentrated into aggregates at nodal or antinodal positions associated with standing SAWs.[28−34] In the latter, the attenuation of the sound wave in the liquid as the

Received: April 24, 2020
Accepted: June 1, 2020
Published: June 1, 2020

ACS Publications © 2020 American Chemical Society

https://dx.doi.org/10.1021/acs.analchem.0c01757
Anal. Chem. 2020, 92, 10024−10032

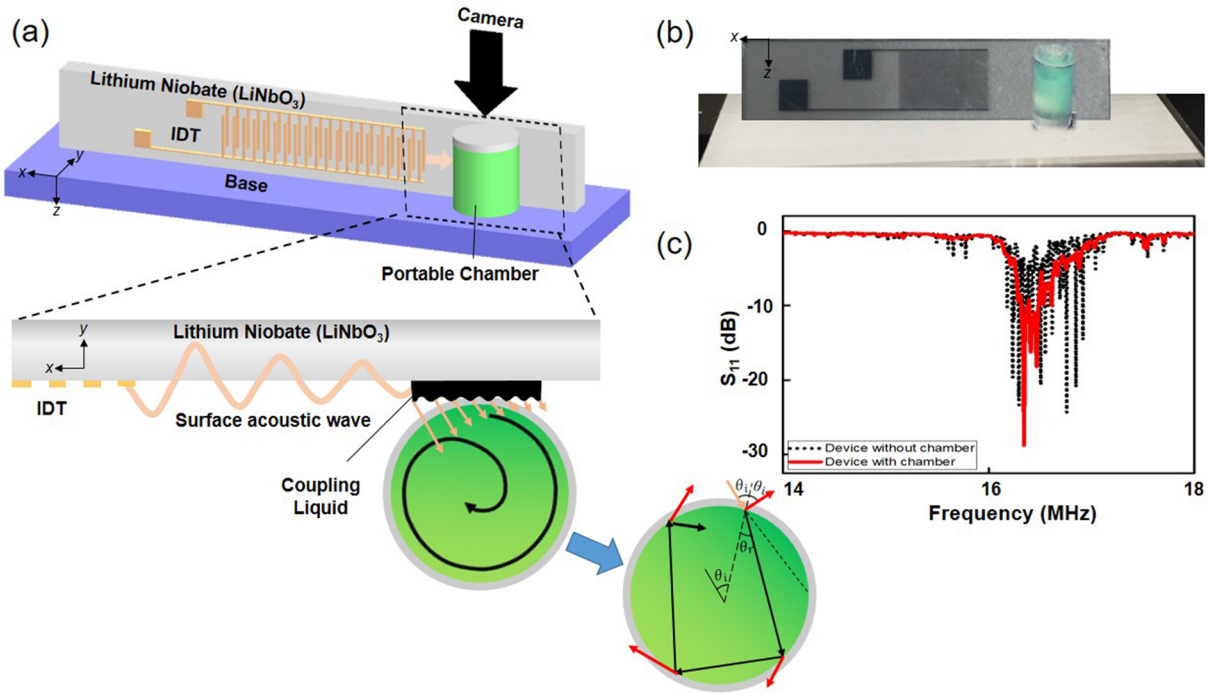

Figure 1. (a) Schematic illustration (not to scale) and (b) image of the experimental setup showing the orthogonal chamber placement configuration to minimize standing wave generation. Also shown in the side image in (a) are brief results from a ray tracing analysis showing the reflection of the wave within the closed chamber. The black and red arrows respectively indicate reflection and transmission of the incident wave, and θ_i and θ_r are the incident and reflected angles. (c) Reflection coefficient S_{11} in the absence (black dashed line) and presence (red solid line) of the fluid and chamber loading.

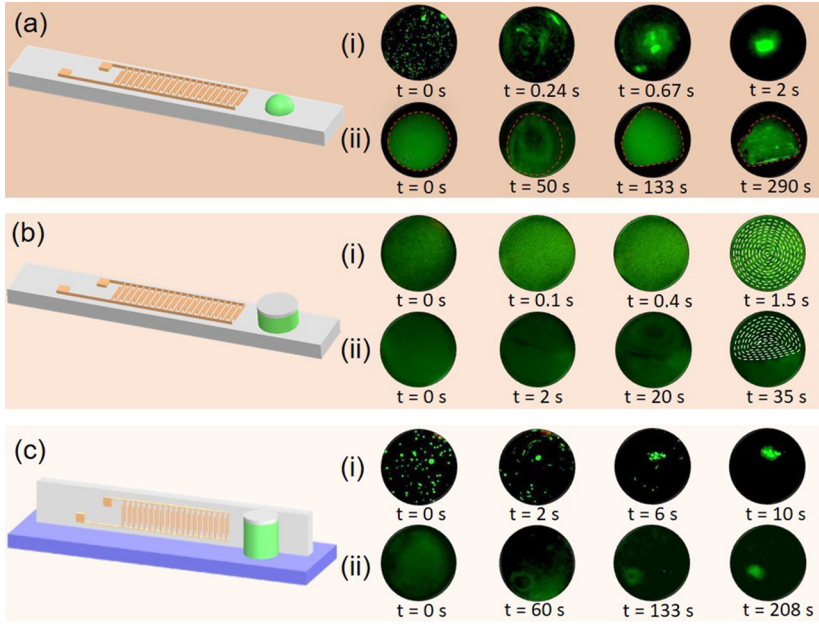

Figure 2. Dynamic behavior of (i) large (6.34 or 10 μm) and (ii) small (1 or 0.3 μm) particles in different chamber configurations under the SAW microcentrifugation flow: (a) conventional open chamber where the sample is subject to evaporation, (b) conventional closed chamber, and (c) the novel chamber configuration proposed in the present work. The input power of the device was fixed at 2.4 W. The red dashed lines in (a-ii) roughly indicate the contact lines of the evaporated drop. In this case, the drop evaporation resulted in significant deformation of the drop contact line. The white dotted lines in (b-i) and (b-ii) guide the visualization of the aggregated particles along the nodes of the standing waves that arise in the closed chamber, as the particles were too small to observe clearly in the image through the closed chamber.

SAW energy leaks into the fluid generates a recirculatory flow known as acoustic streaming. While this has been employed for trapping and aggregating particles and cells in a cross-flow stream within a microchannel transverse to the acoustic streaming flow,[35−38] the vortex region over which the particles can be sampled and within which they concentrate is, however, limited in dimension. In contrast to this localized trapping effect, it is also possible to set up an azimuthal vortical flow

https://dx.doi.org/10.1021/acs.analchem.0c01757
Anal. Chem. 2020, 92, 10024−10032

within a sessile drop that can be used to rapidly and effectively concentrate particles across the bulk of the drop volume in a manner akin to a microcentrifugation effect;[39−44] variations of the technique include the possibility of carrying out the concentration in a drop on a superstrate[45,46] or in a well of a microarray plate[47] by transmitting the SAW energy through a fluid couplant.[48]

Despite their simplicity, a significant limitation of open systems, whether sessile drops or microarray wells, is the susceptibility of the sample to contamination and evaporation. While closed microchannels have been used in conjunction with SAW devices, these have mainly been made out of polydimethylsiloxane (PDMS) for simplicity and suffer from strong acoustic absorption, which not only leads to undesirable heating but also significantly reduces the amount of acoustic energy available to drive the actuation.[49] Moreover, unless the chamber geometry is asymmetric, the reflections off the channel walls and lid due to the strong mismatch in acoustic impedance also results in the generation of standing waves within the chamber.[50,51] Consequently, particles are trapped along the nodes or antinodes of these standing waves, preventing their migration and hence concentration due to the flow. As such, the use of closed setups has typically been limited in practice to systems that only require low acoustic energy and where standing SAWs are desirable and not prohibitive, such as particle alignment and sorting,[13] therefore precluding most SAW microfluidic actuation involving acoustically driven flows, including SAW microcentrifugation.

Here, we propose a novel closed chamber setup machined from poly(methyl methacrylate) (PMMA) that circumvents the aforementioned limitations. Unlike the conventional chamber configuration that has been employed with SAW devices to date in which the cylindrical chamber longitudinal (z) axis is orthogonal to the SAW substrate and SAW propagation direction (for example, see the schematic in Figure 2(b)), the chamber orientation is rotated such that its longitudinal axis is now parallel to the SAW substrate and orthogonal to the SAW propagation direction, as shown in Figures 1(a and b) and 2(c). In this orientation, the asymmetric reflections of the sound waves generated in the chamber along the curved chamber walls are prevented from forming standing waves, which is in contrast to the conventional configuration where standing waves are generated as a consequence of the sound wave reflection off the flat, parallel planes that constitute the substrate and top surface of the chamber. Fluid and chamber loading and heating effects due to the presence of the chamber and hence the sample are further minimized, since the sample is not in direct contact with the SAW substrate; the use of PMMA further prevents sound wave absorption[52] and hence heating given that its acoustic impedance is closer to that of the liquid compared to PDMS.[53] More importantly, we show that by carrying out the particle concentration in a closed system and hence eliminating evaporation effects we are able to achieve submicron particle concentration that has been proven to be elusive in an open system. This is due to their longer concentration times T_c, given that this scales inversely with the square of the particle size a, i.e., $T_c \approx 1/a^2$. In an open system susceptible to evaporation and compounded by heating effects due to the SAW irradiation of the liquid, it is typically difficult to carry out operations beyond 10 s, and as such, only particle concentration down to 1 μm has been demonstrated with SAW microcentrifugation to date.[39−47,54,55] In contrast, we are able to extend T_c up to beyond 2 min, which was sufficient to permit the efficient concentration of 200 nm particles. This not only was thought to be impossible with the conventional open drop or chamber setup due to the drop evaporating before concentration was complete but also was thought to be physically impossible.[44]

MATERIALS AND METHODS

The SAW device comprised a 0.5 mm thick, 6.35 mm wide, and 25.63 mm long single crystal piezoelectric 128° Y−X lithium niobate ($LiNbO_3$) substrate on which a 4.45 mm wide and 7.5 mm long interdigitated transducer (IDT) electrode was patterned via standard lithography and wet etching on 5 nm chromium and 200 nm aluminum sputter-coated layers. The IDT width and finger gap is 60 μm to produce a SAW wavelength of 243.7 μm, which, given the SAW phase velocity in the substrate of 3985 m/s, corresponds to a resonant frequency of 16.35 MHz. To generate the traveling SAW, a sinusoidal electrical signal at this frequency from a signal generator (N9310A, Keysight Technologies Pty. Ltd., Mulgrave, VIC, Australia) and amplifier (ZHL-5W-1+, Mini-Circuits, Brooklyn, NY, USA) was applied to the IDT. The voltage and current were monitored using voltage (RTM-ZP10, Rohde & Schwarz GmbH & Co KG, Munich, Germany) and current (P6022, Tektronix Inc., Beaverton, OR, USA) probes, respectively, and the data was recorded on a digital oscilloscope (RTM 1054, Rohde & Schwarz GmbH & Co KG, Munich, Germany), from which the input power data were calculated. Reflection coefficient (S_{11}) data were acquired using a vector network analyzer (ZNB 4, Rohde & Schwarz GmbH & Co KG, Munich, Germany). To minimize heat build-up, a thermoplastic cooler (MCTE1−19913L-S, Element14 Pty. Ltd., Chester Hill, NSW, Australia) was attached to the rear face of the SAW device.

A sample chamber, 2.5 mm in inner diameter and 4 mm in height with a wall thickness of 0.25 mm, was micromachined (ICP 4030 iMC-P, isel AG, Dermbach, Germany) from PMMA (GF13025652 Sigma-Aldrich Pty. Ltd., Castle Hill, NSW, Australia). A 3 mm diameter circular chamber cover was machined from a microscope coverslip and attached to both ends of the chamber. The closed chamber was mounted approximately 3 mm from the last IDT finger in a lateral configuration, with its longitudinal (z) axis parallel to the SAW substrate and orthogonal to the SAW propagation direction, as depicted in Figure 1(a). This was done such that the chamber wall curvature guides the sound waves along its circumference (for example, see the side image in Figure 1(a)) rather than generating a standing wave within a chamber due to the reflections off parallel flat surfaces between the piezoelectric substrate and the top cover of the chamber in the conventional chamber orientation (for example, see the schematic in Figure 2). An approximately 40 μm thick ultrasonic gel (Sonotech Soundsafe, Andrew Engineering Pty. Ltd., Heidelberg West, VIC, Australia) couplant layer was applied between the SAW device and the chamber to facilitate efficient transmission of the acoustic waves into the chamber. Given that the chamber and sample are not in direct contact with the SAW device, unlike in the conventional setup, loading effects due to the fluid and chamber are minimized, as can be seen from the S_{11} curves in Figure 1(c).

A 0.5 μL suspension of both synthetic particles in 14 μL of Milli-Q water (18.2 MΩ.cm; Merck Millipore, Bayswater, VIC, Australia) and bacterial cells in cell media at a concentration of

https://dx.doi.org/10.1021/acs.analchem.0c01757
Anal. Chem. 2020, 92, 10024−10032

4.5×10^6 particles or cells/mL was employed for the particle concentration experiments. The former comprised 0.2, 0.3, 0.5, 1, 1.82, 6.34, and 10.1 μm polystyrene particles (Polysciences Inc., Warrington, PA, USA). The bacteria consisted of a *Mycoplasma hominis* strain (214/1, RMIT University Culture Collection, Bundoora, VIC, Australia), which are among the smallest spherically shaped bacteria with a diameter of 200−300 nm, as confirmed visually under a microscope (EVOS M5000, Lite Technology Corp., Bothell, WA, USA) and via dynamic light scattering measurements (Zetasizer, Malvern Instruments Ltd., Malvern, UK); the refractive index of the bacteria solution (1.33) was measured using a hand-held refractometer (Refracto 30PX/30GS, Mettler Toledo Ltd., Port Melbourne, VIC, Australia). The bacteria was grown in a mycoplasma broth base (CM0403, Oxoid Ltd., Basingstoke, UK) by dissolving 12.75 g in 500 mL of distilled water sterilized by autoclaving, followed by aseptic addition of filter-sterilized 100 mL of heat-inactivated horse serum (H1270, Sigma-Aldrich Pty. Ltd., Castle-Hill, NSW, Australia), 50 mL of a yeast extract solution (J850, Sigma-Aldrich Pty. Ltd., Castle-Hill, NSW, Australia), and penicillin (P3032, Sigma-Aldrich Pty. Ltd., Castle-Hill, NSW, Australia). The cells were then propagated aerobically at 37 °C and incubated for 3 days, centrifuged, and thrice washed in 1 mL of a phosphate buffer solution (PBS, Sigma-Aldrich Pty. Ltd., Castle-Hill, NSW, Australia). They were subsequently fluorescently labeled through the addition of 100 μL of 300 nM 4′,6-diamidino-2-phenylindole dihydrochloride (DAPI D3571, Sigma-Aldrich Pty. Ltd., Castle-Hill, NSW, Australia), after which they were incubated for 10 min in a dark room at room temperature. Prior to use, the cells were washed and fixed with 4% (wt/vol) formaldehyde (158127, Sigma-Aldrich Pty. Ltd., Castle-Hill, NSW, Australia).

The particle/cell dynamics under the SAW microcentrifugation flow were recorded using a digital video camera (BM-14, Nikon Corp., Tokyo, Japan) at 30 frames/s and a microscope (Leica DM2500, Thermo Fisher Scientific, Bothell, WA, USA). Image frames acquired from the video footage were characterized using ImageJ (1.52p, National Institutes of Health, Bethesda, MD, USA).[56] A rectangular subset of each image comprising an area of around 1000 μm × 175 μm was analyzed, from which the mean-normalized pixel intensity (NPI)[57] was calculated from the average pixel intensity in the selected area. The particle concentration time T_c is defined as the time that the mean NPI decreases to a value of 0.2.

Post-exposure cell viability was conducted through a standard 3-day turbidity test[58,59] in 96-well plates by adding 190 μL of mycoplasma broth into each plate, followed by 10 μL of the control and treated cells. The plate was then incubated aerobically at 37 °C for 1 to 3 days, during which optical density (OD) values of the cell suspension were measured at different time points using a microplate reader (POLARstar Omega, BMG LabTech Pty. Ltd., Mornington, VIC, Australia) at an absorption wavelength of 600 nm. The percentage of cell viability was calculated from $(OD_{treated} - OD_{blank})/(OD_{control} - OD_{blank}) \times 100\%$. Quadruplicate experiments were carried out, and an unpaired *t*-test with a confidence interval of 95% was employed to determine statistical significance between the treated and control samples.

RESULTS AND DISCUSSION

The inability to concentrate submicron particles and below using the conventional SAW microcentrifugation setup comprising either a sessile drop placed on the SAW device (see schematic in Figure 2(a)) or an open chamber atop the device whose longitudinal axis is oriented orthogonal to the SAW substrate and SAW propagation direction has been reported in various studies.[39−47,54,55] In contrast to the behavior of larger micron dimension particles, which rapidly concentrate into a localized cluster, as shown in Figure 2(a-i), particles approximately 1 μm and below can instead be seen to form an annular particle "ring" (Figure 2(a-ii)), at least over the short durations (t = 50 s) reported prior to the evaporation of the drop, which can be seen from its deformed contact line in Figure 2(a-ii). These particle rings were first reported by Destgeer et al.,[44] who attributed them to standing wave effects that oppose and overwhelm the drag force on the particles arising from acoustic streaming that act to concentrate them into a localized aggregate.

We show below that this may not be entirely true, i.e., that it is indeed possible to concentrate smaller micron and submicron particles under SAW microcentrifugation. However, this requires a significantly longer time, given that the concentration period T_c under shear-induced migration effects, which is the dominant mechanism by which the particles traverse streamlines to migrate into a localized aggregate in the center of the drop under the SAW-driven acoustic streaming,[39−42] scales as the inverse of the squared particle size ($T_c \approx 1/a^2$). For a = 1 μm, $T_c \approx R^2/(a^2\dot{\gamma}\varphi) \approx 10^2$ s; here, R is the characteristic radius of the vortex (estimated in the experiments to be approximately 100 μm), $\dot{\gamma}$ is the shear rate (estimated in the experiments to be approximately 10^2 s^{-1}), and φ is the local hard-sphere close-packing fraction (approximately 0.68).[60] As the particle concentration in all of the preceding studies has been carried out in an open system, whether in a sessile drop or an open chamber, a considerable volume of the liquid typically evaporates, exacerbated by the tendency for the SAW to also heat the liquid in direct contact with it, before the concentration can proceed to completion. As such, only the intermediate "ring" states, which form within 10−30 s, have been reported in the literature. No observations have been carried out to date over longer times to show the fate of this particle ring if the SAW microcentrifugation were to be allowed to proceed for longer times, which is probably due to limitations in the total duration over which the experiment can be carried out given the rapidly evaporating drop and, as a consequence, the distortion of its contact line (Figure 2(a-ii)).

With SAW devices, it is, however, not trivial to simply affix a lid to close the chamber in order to minimize evaporation, at least for the configuration that the chamber has been conventionally oriented. Doing so for chamber heights and dimensions comparable or less than the sound wave attenuation length in the liquid leads to the generation of standing sound wave patterns due to multiple reflections of the sound waves between the SAW substrate at the bottom and the lid at the top. This then leads to the tendency of particle trapping at the nodes or antinodes of the standing wave, as shown in Figure 2(b), which, in turn, impedes the action of the hydrodynamics in driving convective migration of the particles into a localized aggregate at the center of the chamber.

By minimizing the generation of standing waves through the introduction of wall curvature along the sound wave propagation and reflection pathway in the chamber with the novel orientation (see, for example, the simple sketch with the ray tracing analysis in the side image in Figure 1(a)), which

https://dx.doi.org/10.1021/acs.analchem.0c01757
Anal. Chem. 2020, 92, 10024−10032

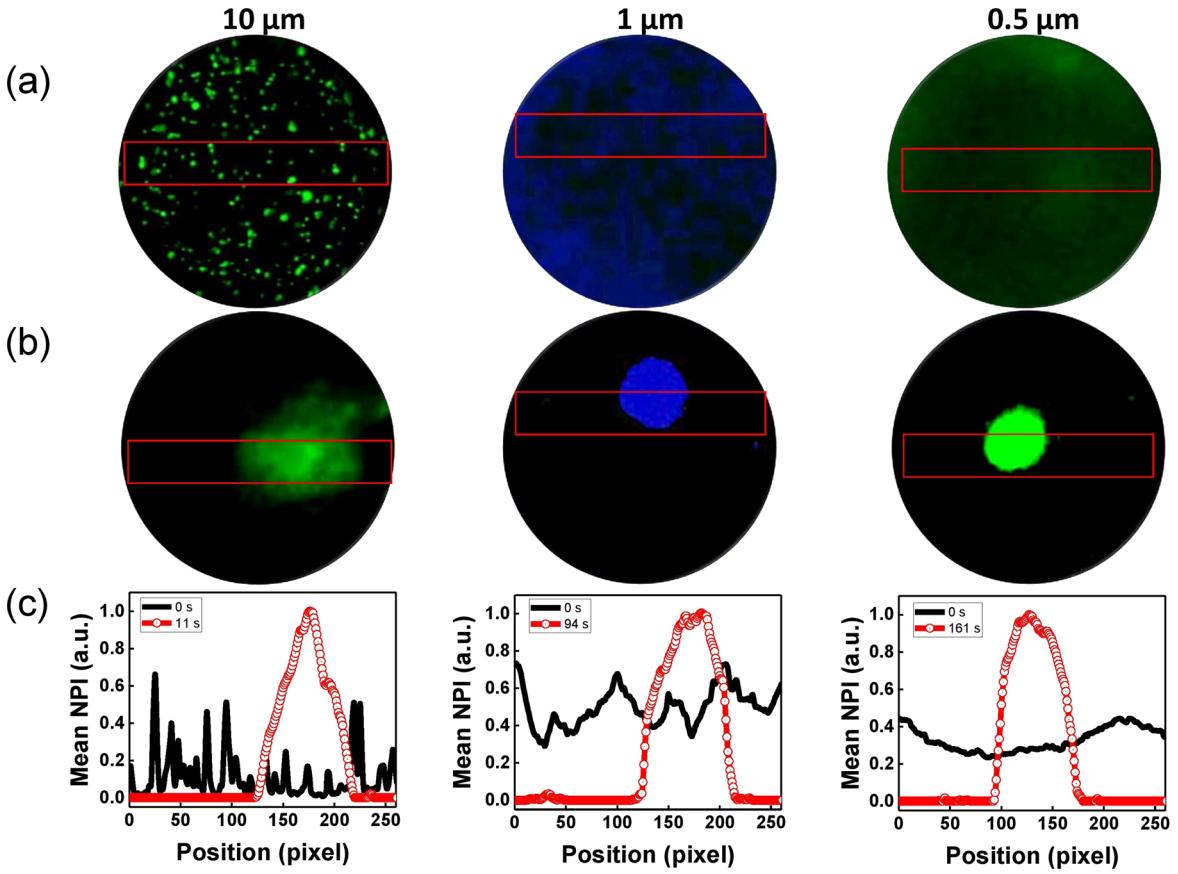

Figure 3. Snapshot images showing the fate of 10, 1, and 0.5 μm particle suspensions in the chamber (a) prior to (i.e., 0 s) and (b) following SAW exposure over a duration of 11, 94, and 161 s, respectively. (c) Averaged normalized pixel intensity (NPI) values over the area defined by the respective highlighted regions prior to (black curves) and following (red curves) SAW exposure. The input power to the device for all of the experiments was fixed at 2.4 W.

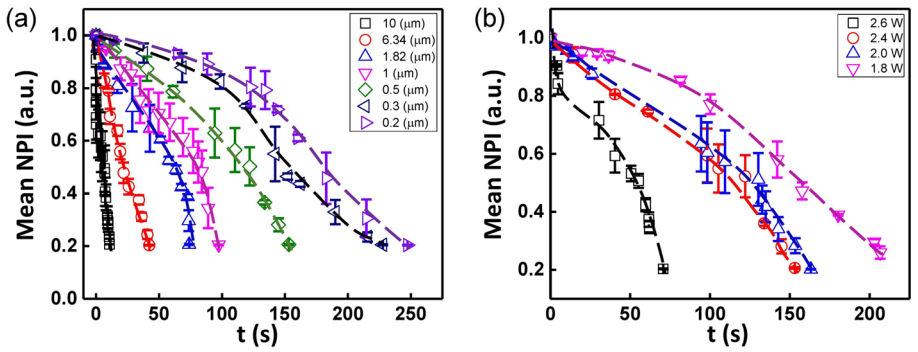

Figure 4. Change in the mean normalized pixel intensity (NPI) with time t for different (a) particle diameters and (b) input powers to the device. In (a), the input power was fixed at 2.4 W whereas in (b) the particle size was fixed at 0.5 μm.

also minimizes heating effects by eliminating direct contact of the chamber and sample with the SAW substrate, we are able to circumvent these limitations to run the particle concentration experiments for longer times. It can be seen from Figures 3 and 4(a) that we were able to efficiently concentrate particles down to 0.2 μm. As expected, the requisite particle concentration time T_c was substantially longer as the particle size a decreased such that the entire duration exceeds 100 s for submicron particles, which would not have been possible for an open chamber experiment where a substantial proportion of the liquid would have evaporated and hence affected the particle dynamics within it. Further, it is possible to reduce the particle concentration time by increasing the input power to the SAW device, as seen in Figure 4(b). For example, the concentration time was reduced by more than 2-fold from over 206 to 70 s for 0.5 μm particles simply by increasing the power by approximately 45% from 1.8 to 2.6 W. However, this would not be an option to achieve submicron particle concentration in the conventional chamber setup in Figure 2(a) since increasing the input power would lead to additional heating, which, in turn, would accelerate the evaporation of the sample. Results of a parametric study investigating different diameter chambers and the effect of the diffraction pattern by placing a 4 mm chamber on a different area of the delay line can be found in Figures S1 and S2.

https://dx.doi.org/10.1021/acs.analchem.0c01757
Anal. Chem. 2020, 92, 10024−10032

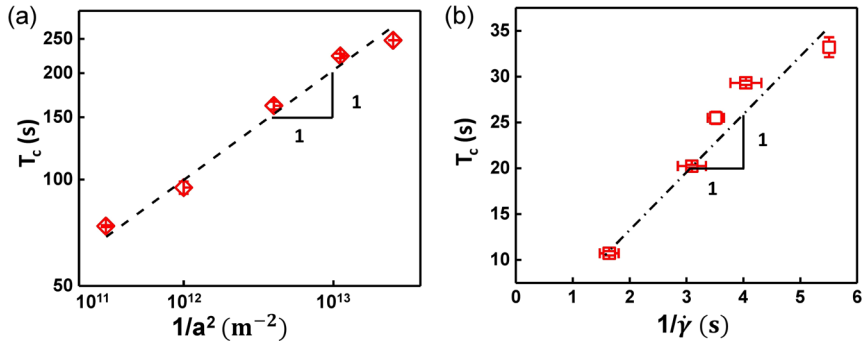

Figure 5. Relationship between the particle concentration time T_c and (a) the particle diameter a and (b) the shear rate $\dot{\gamma}$. In (a), the input power to the device was held at 2.4 W whereas in (b) the particle diameter was held at 10 μm.

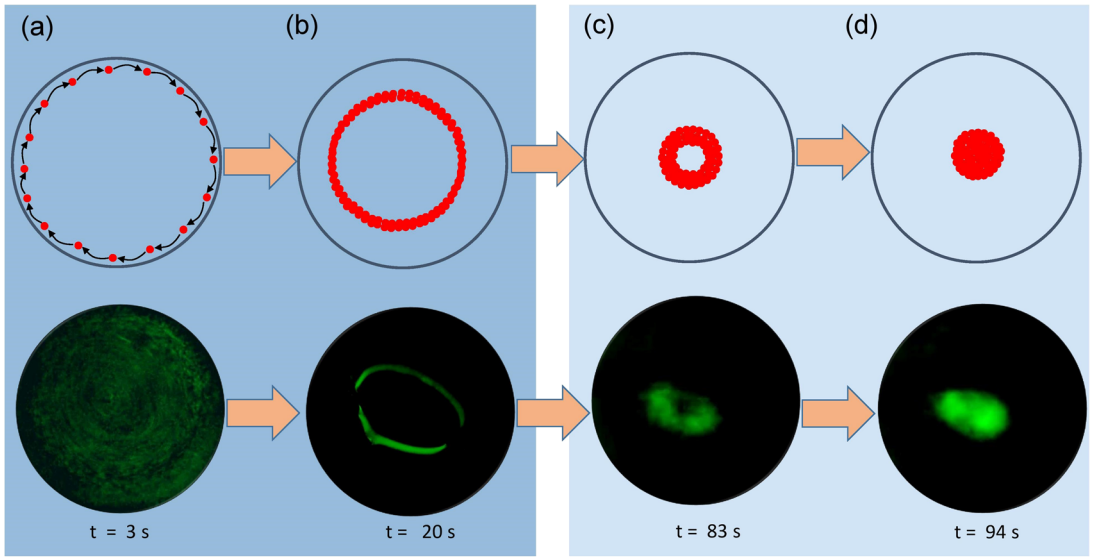

Figure 6. Schematic depiction (top row) and experimental snapshots (bottom row) illustrating the concentration dynamics of small ($\lesssim$ 1 μm) particles due to shear-induced migration arising under the SAW microcentrifugation flow. (a and b) Initial behavior of the particles, which follow the trajectory of the azimuthal flow such that they are taken up into a concentric streamline associated with the flow so as to pack and form an intermediate ring-like structure. This typically occurs within the first 20 to 40 s, depending on the particle diameter, and was observed in the experiments of Destgeer et al.[44] (c and d) Subsequent long-term behavior, where the ring is subsequently concentrated into a local aggregated cluster, which was not observed by Destgeer et al.,[44] as they had terminated their experiments early at times of around 20 to 30 s.

From Figure 5, it would appear that, regardless of the particle size, the fundamental physical mechanism by which the particles are driven to concentrate in the new chamber configuration remains similar to that in the conventional setup,[39,40,55] other than the underlying rotational streaming flow occurring axisymmetrically about the transverse (y) axis as opposed to the vertical (z) axis. More specifically, the particles are initially drawn into the dominant concentric flow streamlines associated with the azimuthal microcentrifugation flow and pack into an intermediate ring-like structure, as observed in Figure 6(a). This is consistent with other previous SAW microcentrifugation experiments,[39,40,55] as well as that driven by other external forces under the same microcentrifugation flow dynamics starting from an initial dilute particle suspension (see, for example, ref 61); however, we note that the intermediate ring state appears to be more prominent for smaller particles given the longer overall concentration times. Once a local hard-sphere close-packing fraction (approximately $\varphi = 0.68$) in the ring is achieved, cross-streamline particle transport then ensues due to multiparticle interactions at a rate of $\dot{\gamma}\varphi a^2$ across the shear gradient from the high shear region at the periphery of the chamber to the center of the chamber, concentrating the particles into a dense local aggregated cluster,[60] as observed in Figure 6(b). This is supported by the $1/a^2$ and $1/\dot{\gamma}$ scaling for the particle concentration time T_c observed in Figure 5, even for the small submicron particles, which is consistent with the time $T_c \approx R^2/a^2\dot{\gamma}\varphi$ it takes for the particles to diffuse into a vortex of radius R under the influence of the shear gradient. In any case, we note that the intermediate ring state in Figure 6(a) is consistent with that observed by Destgeer et al.[44] who terminated their experiments without allowing the concentration to proceed to its completion in Figure 6(b).

Finally, we demonstrate the practical utility of the device for the concentration of real submicron particles using the smallest known antibiotic-resistant bacterium *M. hominis*, with sizes between 200 to 300 nm (Figure 7(d)). *M. hominis* is known to be the cause of severe genitourinary (e.g., urethritis and bacterial vaginosis) and respiratory tract infections. Given that the bacterium does not possess the typical bacterial peptidoglycan cell wall, it cannot be visualized on bacterial gram stains.[62] As such, concentrating it efficiently is an

https://dx.doi.org/10.1021/acs.analchem.0c01757
Anal. Chem. 2020, 92, 10024−10032

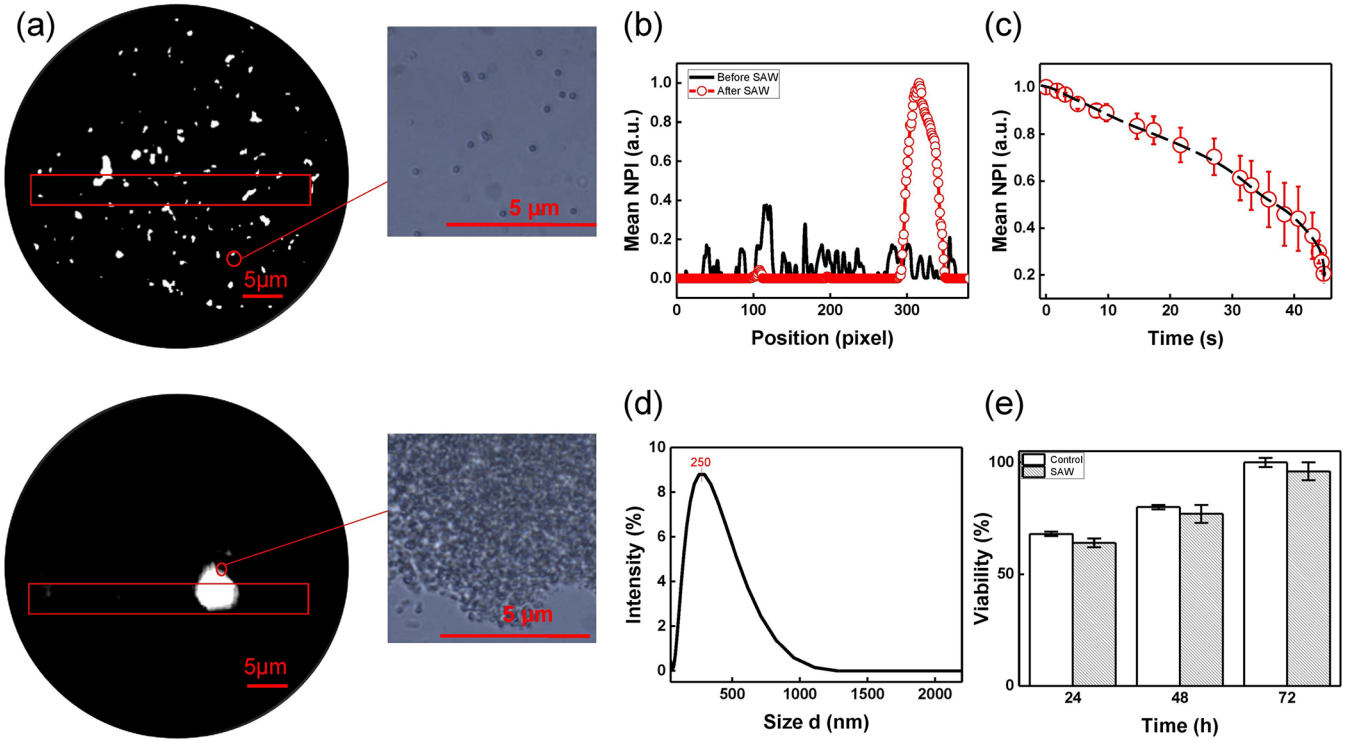

Figure 7. (a) Optical microscopic images (color inverted during postprocessing) showing a suspension of *M. hominis* in the chamber prior to (top) and following (bottom) SAW microcentrifugation, demonstrating the possibility for driving the concentration of these submicron bioparticles under the flow with the transverse closed chamber configuration in Figure 1(a). This is further evidenced by the absence and subsequent presence of the localized particle aggregates in the magnified insets and verified by (b) the averaged normalized pixel intensity (NPI) values over the area defined by the respective highlighted regions and (c) a plot showing the change in the mean normalized pixel intensity (NPI) with time *t*. (d) Size distribution of the *M. hominis* sample, as measured via dynamic light scattering. (e) Cell viabilities of untreated cells (control) and those exposed to the SAW microcentrifugation over a 72 h period, as measured from standard turbidity measurements.

important step for its detection in disease diagnosis. Figure 7(a–c) shows the efficient concentration of the bacterial cells in just 44 s under the SAW microcentrifugation flow with the transverse chamber configuration in Figure 1(a). Further, we also verified from a 3 day turbidity test that the majority of the bacteria remained viable (94% compared to 100% in the unexposed control after 72 h) and continued to proliferate normally following exposure to the SAW irradiation and hydrodynamic shear associated with the SAW microcentrifugation flow (Figure 7(e)), which is consistent with previous work where SAW exposure, even at much higher powers, was shown to have minimal adverse effects on cell viability, proliferation, and even differentiation.[63−66]

CONCLUSION

While SAW microcentrifugation has long been demonstrated as a powerful means for driving efficient microfluidic particle concentration, this has to date been largely confined to particles larger than 1 μm. Our previous studies together with others have highlighted the difficulties in concentrating smaller particles of 1 μm and below. Rather than concentrating into a tight and aggregated local cluster, as is observed for larger particles, a ring-like aggregate is instead obtained for smaller ($\leq$1 μm) particles.[44] We assert in this work, however, that these particle rings are not the final fate of the particles under the SAW microcentrifugation flow but that they are only an intermediate state that studies to date have not progressed beyond to achieve complete particle concentration into a localized cluster over longer durations. We speculate that this is because the studies on SAW microcentrifugation to date have been carried out in open systems, whether a sessile drop on the SAW device or an open-top chamber placed on the SAW device. Given that the particles concentrate due to a shear diffusion mechanism, the concentration time increases as the inverse of the squared particle size, and hence, the time required for the SAW microcentrifugation flow to achieve full particle concentration rapidly increases as the particle size decreases. It is, therefore, likely that the studies to date were only carried out over short durations (typically 10−30 s) over which evaporation was not significant, and hence, the experiments did not progress beyond the durations over which the particle rings were obtained.

As a consequence of the standing waves being generated due to multiple reflections of the sound waves in the chamber, it is not simply trivial to place a lid over the conventional SAW microcentrifugation chamber setup to close it so as to eliminate evaporation effects. Doing so merely led to particle trapping along the nodal or antinodal lines associated with the standing waves, which prevent the particles from migrating under the microcentrifugation flow and hence the shear gradients to concentrate. As such, we redesigned the SAW microcentrifugation setup in this work to accommodate a novel closed chamber configuration. In addition to eliminating evaporation in the closed setup, the transverse orientation of the chamber, which is contrary and counterintuitive to the conventional upright chamber orientation, prevents the formation of standing waves, as the curved chambers walls in the pathway of the sound wave propagation redistributes and

https://dx.doi.org/10.1021/acs.analchem.0c01757
Anal. Chem. 2020, 92, 10024−10032

disperses the sound wave reflections. Unlike the conventional chamber setup, the present chamber and hence the liquid sample are also not in direct contact with the SAW device but rests atop a fluid coupling layer, therefore minimizing mass loading as well as sample heating effects. Furthermore, we note that only a single IDT set is required to drive the SAW microcentrifugation, unlike some previous studies where a dual offset IDT pair is required to produce the asymmetric SAW required to drive the microcentrifugation; we note that while a single IDT set, placed offset to the drop or chamber, has been reported,[39,40] this requires a significantly larger device footprint, which increases device costs and makes integration difficult.

With this novel chamber configuration, we demonstrate efficient generation of the SAW microcentrifugation flow that is axisymmetric about the transverse axis parallel to the SAW substrate and orthogonal to the SAW propagation direction. With the elimination of evaporation, we show that it is possible to drive the microcentrifugation effect for longer durations by over an order of magnitude, which is sufficient to progress the particle dynamics beyond the intermediate particle "ring" state to achieve complete concentration of micron and submicron particles and cells down to 200 nm in dimension into a localized cluster.

■ ASSOCIATED CONTENT

Supporting Information

The Supporting Information is available free of charge at https://pubs.acs.org/doi/10.1021/acs.analchem.0c01757.

Figure S1, particle concentration dynamics for different chamber diameters C_d with a 6.34 μm polystyrene particle suspension, and Figure S2, images showing streaming patterns for different chamber locations with respect to the IDT for the concentration of 10 μm polystyrene particles inside a 4 mm chamber (PDF)

■ AUTHOR INFORMATION

Corresponding Author

Amgad R. Rezk − *Micro/Nanophysics Research Laboratory, School of Engineering, RMIT University, Melbourne, Victoria 3001, Australia;* orcid.org/0000-0002-3556-5621; Email: amgad.rezk@rmit.edu.au

Authors

Asma Akther − *Micro/Nanophysics Research Laboratory, School of Engineering, RMIT University, Melbourne, Victoria 3001, Australia*

Susan Marqus − *Micro/Nanophysics Research Laboratory, School of Engineering, RMIT University, Melbourne, Victoria 3001, Australia*

Leslie Y. Yeo − *Micro/Nanophysics Research Laboratory, School of Engineering, RMIT University, Melbourne, Victoria 3001, Australia;* orcid.org/0000-0002-5949-9729

Complete contact information is available at: https://pubs.acs.org/10.1021/acs.analchem.0c01757

Notes

The authors declare no competing financial interest.

■ ACKNOWLEDGMENTS

This work was partially carried out at the RMIT MicroNano Research Facility (MNRF), which comprises part of the Victorian Node of the Australian National Fabrication Facility (ANFF). L.Y.Y. gratefully acknowledges funding from the Australian Research Council (ARC) through Discovery Project (DP170101061). The authors also wish to acknowledge the technical help of Ms. Helen Williams and Mr. Adam Vogrin at the PC2 and microscopy facilities in the School of Science.

■ REFERENCES

(1) Sackmann, E. K.; Fulton, A. L.; Beebe, D. J. *Nature* **2014**, *507*, 181−189.
(2) Franke, T. A.; Wixforth, A. *ChemPhysChem* **2008**, *9*, 2140−2156.
(3) Yeo, L. Y.; Chang, H.-C.; Chan, P. P. Y.; Friend, J. R. *Small* **2011**, *7*, 12−48.
(4) Nilsson, J.; Evander, M.; Hammarström, B.; Laurell, T. *Anal. Chim. Acta* **2009**, *649*, 141−157.
(5) Karimi, A.; Yazdi, S.; Ardekani, A. M. *Biomicrofluidics* **2013**, *7*, 021501.
(6) Sajeesh, P.; Sen, A. *Microfluid. Nanofluid.* **2014**, *17*, 1−52.
(7) Ahmed, H.; Ramesan, S.; Lee, L.; Rezk, A. R.; Yeo, L. Y. *Small* **2020**, *16*, 1903605.
(8) Kang, Y.; Li, D. *Microfluid. Nanofluid.* **2009**, *6*, 431−460.
(9) Pethig, R. *Biomicrofluidics* **2010**, *4*, 022811.
(10) Chang, H.-C.; Yeo, L. Y. *Electrokinetically Driven Microfluidics and Nanofluidics*; Cambridge University, 2010.
(11) Harrison, H.; Lu, X.; Patel, S.; Thomas, C.; Todd, A.; Johnson, M.; Raval, Y.; Tzeng, T.-R.; Song, Y.; Wang, J.; Li, D.; Xuan, X. *Analyst* **2015**, *140*, 2869−2875.
(12) Friend, J.; Yeo, L. *Rev. Mod. Phys.* **2011**, *83*, 647−704.
(13) Lin, S.-C. S.; Mao, X.; Huang, T. J. *Lab Chip* **2012**, *12*, 2766−2770.
(14) Baudoin, M.; Thomas, J.-L. *Annu. Rev. Fluid Mech.* **2020**, *52*, 205−234.
(15) Meng, L.; Cai, F.; Li, F.; Zhou, W.; Niu, L.; Zheng, H. *J. Phys. D: Appl. Phys.* **2019**, *52*, 273001.
(16) Grier, D. G. *Nature* **2003**, *424*, 810−816.
(17) Mishra, A.; Kwon, J.-S.; Thakur, R.; Wereley, S. *Trends Biotechnol.* **2014**, *32*, 414−421.
(18) Lim, J.; Lanni, C.; Evarts, E. R.; Lanni, F.; Tilton, R. D.; Majetich, S. A. *ACS Nano* **2011**, *5*, 217−226.
(19) Forbes, T. P.; Forry, S. P. *Lab Chip* **2012**, *12*, 1471−1479.
(20) Ramadan, Q.; Samper, V.; Poenar, D. P.; Yu, C. *Biosens. Bioelectron.* **2006**, *21*, 1693−1702.
(21) Hejazian, M.; Nguyen, N.-T. *Biomicrofluidics* **2016**, *10*, 044103.
(22) Connacher, W.; Zhang, N.; Huang, A.; Mei, J.; Zhang, S.; Gopesh, T.; Friend, J. *Lab Chip* **2018**, *18*, 1952−1996.
(23) White, R. M.; Voltmer, F. W. *Appl. Phys. Lett.* **1965**, *7*, 314−316.
(24) Rezk, A. R.; Tan, J. K.; Yeo, L. Y. *Adv. Mater.* **2016**, *28*, 1970−1975.
(25) Ding, X.; Li, P.; Lin, S.-C. S.; Stratton, Z. S.; Nama, N.; Guo, F.; Slotcavage, D.; Mao, X.; Shi, J.; Costanzo, F.; Huang, T. J. *Lab Chip* **2013**, *13*, 3626−3649.
(26) Destgeer, G.; Sung, H. J. *Lab Chip* **2015**, *15*, 2722−2738.
(27) Go, D. B.; Atashbar, M. Z.; Ramshani, Z.; Chang, H.-C. *Anal. Methods* **2017**, *9*, 4112−4134.
(28) Nam, J.; Lim, H.; Kim, D.; Shin, S. *Lab Chip* **2011**, *11*, 3361−3364.
(29) Chen, Y.; Li, S.; Gu, Y.; Li, P.; Ding, X.; Wang, L.; McCoy, J. P.; Levine, S. J.; Huang, T. J. *Lab Chip* **2014**, *14*, 924−930.
(30) Ahmed, H.; Destgeer, G.; Park, J.; Jung, J. H.; Ahmad, R.; Park, K.; Sung, H. J. *Anal. Chem.* **2017**, *89*, 13575−13581.
(31) Nguyen, T. D.; Tran, V. T.; Fu, Y. Q.; Du, H. *Appl. Phys. Lett.* **2018**, *112*, 213507.
(32) Habibi, R.; Neild, A. *Lab Chip* **2019**, *19*, 3032−3044.
(33) Richard, C.; Fakhfouri, A.; Colditz, M.; Striggow, F.; Kronstein-Wiedemann, R.; Tonn, T.; Medina-Sánchez, M.; Schmidt, O. G.; Gemming, T.; Winkler, A. *Lab Chip* **2019**, *19*, 4043−4051.

(34) Sazan, H.; Piperno, S.; Layani, M.; Magdassi, S.; Shpaisman, H. *J. Colloid Interface Sci.* **2019**, *536*, 701−709.
(35) Collins, D. J.; Ma, Z.; Ai, Y. *Anal. Chem.* **2016**, *88*, 5513−5522.
(36) Collins, D. J.; Ma, Z.; Han, J.; Ai, Y. *Lab Chip* **2017**, *17*, 91−103.
(37) Collins, D. J.; Khoo, B. L.; Ma, Z.; Winkler, A.; Weser, R.; Schmidt, H.; Han, J.; Ai, Y. *Lab Chip* **2017**, *17*, 1769−1777.
(38) Mao, Z.; Li, P.; Wu, M.; Bachman, H.; Mesyngier, N.; Guo, X.; Liu, S.; Costanzo, F.; Huang, T. J. *ACS Nano* **2017**, *11*, 603−612.
(39) Li, H.; Friend, J. R.; Yeo, L. Y. *Biomed. Microdevices* **2007**, *9*, 647−656.
(40) Shilton, R.; Tan, M. K.; Yeo, L. Y.; Friend, J. R. *J. Appl. Phys.* **2008**, *104*, 014910.
(41) Raghavan, R. V.; Friend, J. R.; Yeo, L. Y. *Microfluid. Nanofluid.* **2010**, *8*, 73−84.
(42) Rogers, P. R.; Friend, J. R.; Yeo, L. Y. *Lab Chip* **2010**, *10*, 2979−2985.
(43) Destgeer, G.; Jung, J. H.; Park, J.; Ahmed, H.; Sung, H. J. *Anal. Chem.* **2017**, *89*, 736−744.
(44) Destgeer, G.; Cho, H.; Ha, B. H.; Jung, J. H.; Park, J.; Sung, H. J. *Lab Chip* **2016**, *16*, 660−667.
(45) Reboud, J.; Auchinvole, C.; Syme, C. D.; Wilson, R.; Cooper, J. M. *Chem. Commun.* **2013**, *49*, 2918−2920.
(46) Bourquin, Y.; Syed, A.; Reboud, J.; Ranford-Cartwright, L. C.; Barrett, M. P.; Cooper, J. M. *Angew. Chem., Int. Ed.* **2014**, *53*, 5587−5590.
(47) Rezk, A. R.; Ramesan, S.; Yeo, L. Y. *Lab Chip* **2018**, *18*, 406−411.
(48) Hodgson, R. P.; Tan, M.; Yeo, L.; Friend, J. *Appl. Phys. Lett.* **2009**, *94*, 024102.
(49) Langelier, S. M.; Yeo, L. Y.; Friend, J. *Lab Chip* **2012**, *12*, 2970−2976.
(50) Tan, M. K.; Tjeung, R.; Ervin, H.; Yeo, L. Y.; Friend, J. *Appl. Phys. Lett.* **2009**, *95*, 134101.
(51) Johansson, L.; Enlund, J.; Johansson, S.; Katardjiev, I.; Wiklund, M.; Yantchev, V. *J. Micromech. Microeng.* **2012**, *22*, 025018.
(52) Akther, A.; Castro, J. O.; Mousavi Shaegh, S. A.; Rezk, A. R.; Yeo, L. Y. *Soft Matter* **2019**, *15*, 4146−4152.
(53) Yiannacou, K. C. Two Dimensional Acoustofluidic Manipulation of Microparticles. M.Sc. thesis, Tampere University, Tampere, Finland, 2019.
(54) Kishor, R.; Ma, Z.; Sreejith, S.; Seah, Y. P.; Wang, H.; Ai, Y.; Wang, Z.; Lim, T.-T.; Zheng, Y. *Sens. Actuators, B* **2017**, *252*, 568−576.
(55) Sudeepthi, A.; Sen, A. K.; Yeo, L. *Microfluid. Nanofluid.* **2019**, *23*, 76.
(56) Schindelin, J.; et al. *Nat. Methods* **2012**, *9*, 676−682.
(57) Meng, L.; Cai, F.; Jin, Q.; Niu, L.; Jiang, C.; Wang, Z.; Wu, J.; Zheng, H. *Sens. Actuators, B* **2011**, *160*, 1599−1605.
(58) Robertson, J.; Gomersall, M.; Gill, P. *J. Bacteriol.* **1975**, *124*, 1007−1018.
(59) Kundsin, R. B.; Parreno, A.; Poulin, S. *J. Clin. Microbiol.* **1978**, *8*, 445−453.
(60) Leighton, D.; Acrivos, A. *J. Fluid Mech.* **1987**, *181*, 415−439.
(61) Yeo, L. Y.; Hou, D.; Maheshswari, S.; Chang, H.-C. *Appl. Phys. Lett.* **2006**, *88*, 233512.
(62) Mattila, P. S.; Carlson, P.; Sivonen, A.; Savola, J.; Luosto, R.; Salo, J.; Valtonen, M. *Clin. Infect. Dis.* **1999**, *29*, 1529−1537.
(63) Li, H.; Friend, J.; Yeo, L.; Dasvarma, A.; Traianedes, K. *Biomicrofluidics* **2009**, *3*, 034102.
(64) AlHasan, L.; Qi, A.; Rezk, A. R.; Yeo, L. Y.; Chan, P. P. Y. *Integr. Biol.* **2016**, *8*, 12−20.
(65) Castro, J. O.; Ramesan, S.; Rezk, A. R.; Yeo, L. Y. *Soft Matter* **2018**, *14*, 5721−5727.
(66) Ramesan, S.; Rezk, A. R.; Dekiwadia, C.; Cortez-Jugo, C.; Yeo, L. Y. *Nanoscale* **2018**, *10*, 13165−13178.

https://dx.doi.org/10.1021/acs.analchem.0c01757
Anal. Chem. 2020, 92, 10024−10032